

# Photophysical Characterization and Biointeractions of NIR Squaraine Dyes for in Vitro and in Vivo Bioimaging

Sai Kiran Mavileti, Galyna Bila, Valentyn Utko, Evgenia Bila, Tamaki Kato, Rostyslav Bilyy,\* and Shyam S. Pandey\*



Cite This: *ACS Appl. Bio Mater.* 2024, 7, 416–428



Read Online

ACCESS |



Metrics & More



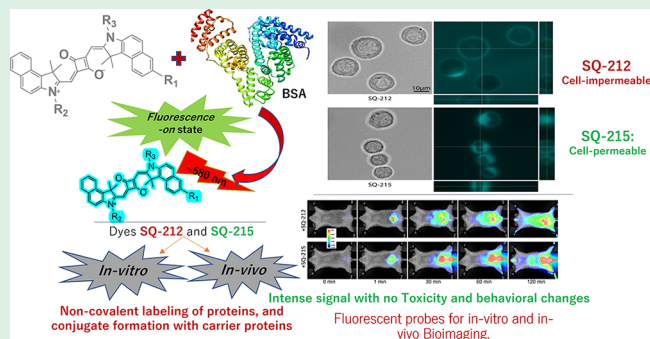
Article Recommendations



Supporting Information

**ABSTRACT:** The increasing demand for reliable near-infrared (NIR) probes exhibiting enduring fluorescence in living systems and facile compatibility with biomolecules such as peptides, antibodies or proteins is driven by the increasing use of NIR imaging in clinical diagnostics. To address this demand, a series of carboxy-functionalized unsymmetrical squaraine dyes (SQ-27, SQ-212, and SQ-215) along with non-carboxy-functionalized SQ-218 absorbing and emitting in the NIR wavelength range were designed and synthesized followed by photophysical characterization. This study focused on the impact of structural variations in the alkyl chain length, carboxy functionality positioning, and spacer chain length on dye aggregation and interaction with bovine serum albumin (BSA) as a model protein. In phosphate buffer (PB), the absorption intensity of the dyes markedly decreased accompanied by pronounced shoulders indicative of dye aggregation, and complete fluorescence quenching was seen in contrast to organic solvents. However, in the presence of BSA in PB, there was an enhancement in absorption intensity while regaining the fluorescence coupled with a remarkable increase in the intensity with increasing BSA concentrations, signifying the impact of dye–BSA interactions on preventing aggregation. Further analysis of Job's plot unveiled a 2:1 interaction ratio between BSA and all dyes, while the binding studies revealed a robust binding affinity ( $K_a$ ) in the order of  $10^7$ /mol. SQ-212 and SQ-215 were further tested for their in vitro and in vivo imaging capabilities. Notably, SQ-212 demonstrated nonpermeability to cells, while SQ-215 exhibited easy penetration and prominent cytoplasmic localization in in vitro studies. Injection of the dyes into laboratory mice showcased their efficacy in visualization, displaying stable and intense fluorescence in tissues without toxicity, organ damage, or behavioral changes. Thus, SQ-212 and SQ-215 are promising candidates for imaging applications, holding potential for noninvasive cellular and diagnostic imaging as well as biomarker detection when coupled with specific vectors in living systems.

**KEYWORDS:** Squaraine dyes, BSA interaction, Dye aggregation, Noncovalent labeling, in vitro & in vivo Bioimaging



## 1. INTRODUCTION

The use of bioimaging techniques allows for non-invasive and real-time visualization of biological processes within tissues and internal organs, offering qualitative and quantitative insights at the cellular or molecular level. In comparison to traditional imaging methods such as magnetic resonance imaging (MRI), ultrasound imaging, X-ray, computed tomography (CT scan), and radionuclide imaging, optical imaging has emerged as a highly advantageous technique in medical research. This is due to its exceptional attributes, including high spatial resolution, portability, real-time display, heightened sensitivity, cost-effectiveness, and a non-invasive nature.<sup>1,2</sup> Fluorescent probes offer valuable insights into the role of biomolecules and can be designed to target and study specific organelles under both healthy and diseased conditions. Fluorescence-based imaging has been employed in the past.<sup>3,4</sup> Fluorescence emission in the near-infrared (NIR) region bears profound significance as

significant interest in this arena has increased, pertaining to sensing, noncovalent binding, and imaging.<sup>5–7</sup> Over the past decade, the development of highly effective fluorescence imaging probes, including organic dyes, quantum dots (QDs), fluorescent proteins/peptide conjugates, nanomaterials, and carbon dots, has garnered significant interest. However, certain limitations such as high photobleaching rates, poor signal-to-noise ratio, short luminescence lifetimes, and limited biocompatibility hinder progress in developing fluorescent probes. This can be overcome by utilizing

**Received:** October 25, 2023  
**Revised:** November 26, 2023  
**Accepted:** November 30, 2023  
**Published:** December 19, 2023



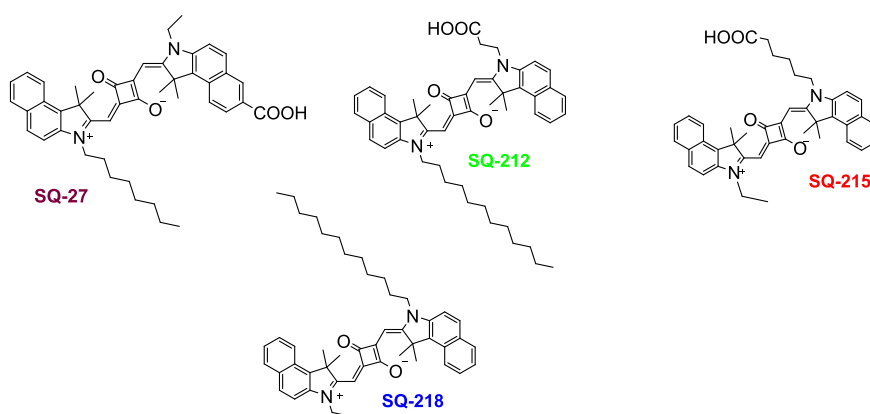


**Figure 1.** Molecular structure of the carboxy-functionalized unsymmetrical squaraine dyes under investigation with varying alkyl chain lengths, spacer lengths, and positions of the carboxy group.

wavelength-tunable dyes that can absorb and emit light in the near-infrared (NIR) region of the electromagnetic spectrum. The emission in the visible range is plagued naturally by the autofluorescence of inherent biomolecules and certain proteins, leading to a large background noise, severe light scattering, a reduced signal-to-noise ratio, and shallow penetration depth, resulting in a low imaging quality. Hence, compounds absorbing and emitting in the NIR region offer higher sensitivity, deeper tissue penetration, low light scattering, and a lower signal-to-noise ratio due to the absence of biomolecules' natural autofluorescence.<sup>8–10</sup> These advantages have propelled the exploration and development of NIR probes for a wide range of biomedical and scientific purposes. Harnessing the potential of NIR fluorescence for improved sensitivity, specificity, and selectivity in areas such as biological sensing, molecular imaging, drug delivery, and biomarker detection has grown manifoldly. Great attention has been given to applying NIR probes in several areas of biosensing and bioimaging, including tissue perfusion, vascular mapping, inflammation monitoring, tumor diagnosis and imaging,<sup>11,12</sup> and for various clinical and preclinical diagnoses and monitoring.<sup>13–16</sup>

The squaraine class of dyes is characterized by their unique aromatic four-membered ring core (3,4-dihydroxycyclobut-3-ene-1,2-dione) derived from squaric acid linked by aromatic heterocyclic moieties at either end, leading to a donor–acceptor–donor molecular arrangement. Their application as fluorescent labels or probes for sensing and imaging research is of significant interest because their wavelength tunable capabilities make them absorb and emit from visible to NIR wavelength regions.<sup>17,18</sup> Squaraine dyes also possess high molar absorptivity and reasonably good quantum yields<sup>19</sup> and good photostability.<sup>20–22</sup> By rational molecular design, squaraine dye's absorption and emission wavelengths can be tuned from the visible to IR wavelength, making them suitable for sensing and imaging.<sup>23</sup> Thus, squaraine dyes with their unique chemical and physical properties find themselves as NIR-fluorescent probes in a plethora of applications such as environmental sensing,<sup>24</sup> molecular sensing,<sup>25,26</sup> bioimaging,<sup>27–29</sup> and biochemical labeling.<sup>30,31</sup> However, their application under physiological conditions is limited by factors such as intrinsic chemical instability and self-aggregation. The fluorescence intensities of squaraine dyes are significantly compromised due to aggregation, leading to even complete quenching. Therefore, dye interactions with serum proteins

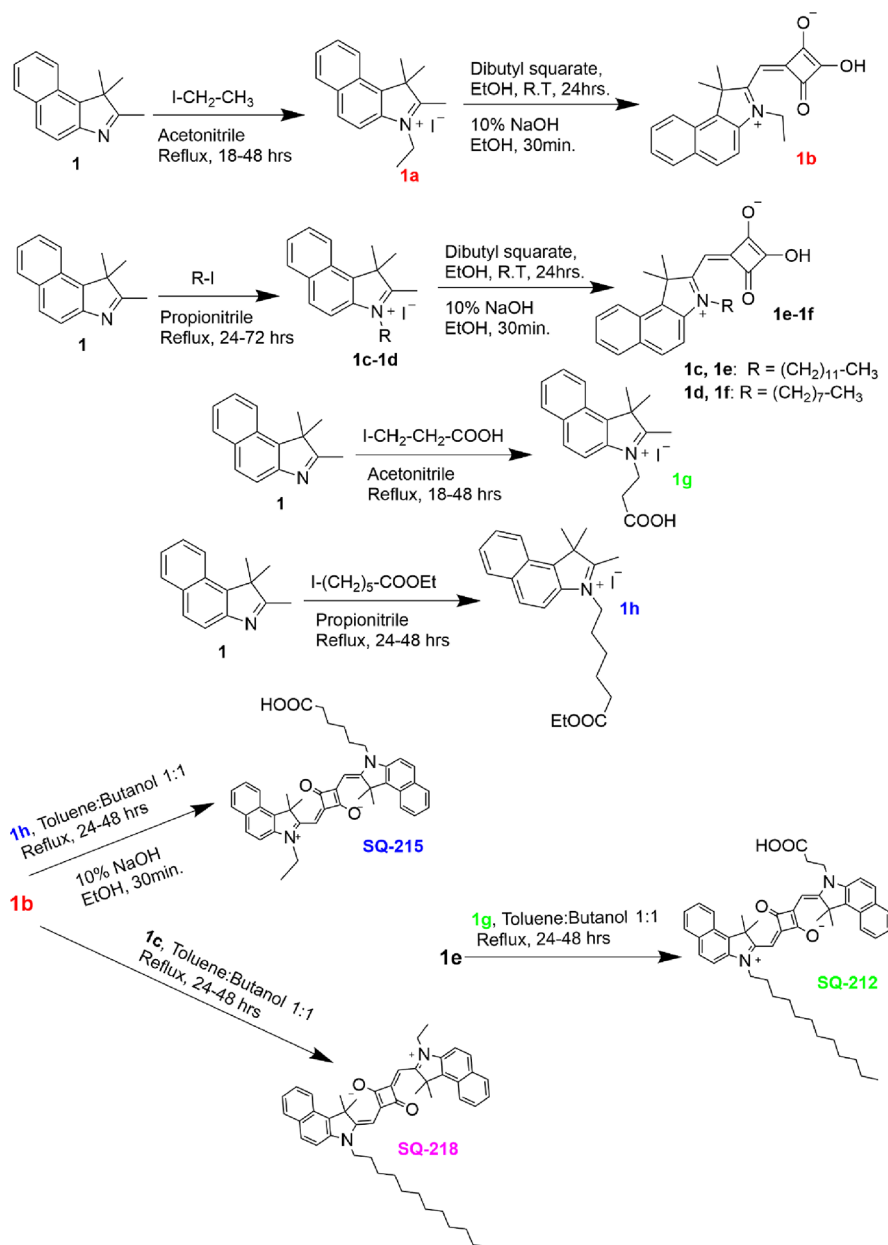
such as BSA and HSA under physiological conditions have been studied to overcome this problem.<sup>32–34</sup>

This work reports the synthesis, characterization, and photophysical studies of four new unsymmetrical squaraine dyes (SQ-27, SQ-212, SQ-215, and SQ-218), as shown in Figure 1. With the exception of SQ-218, the other squaraine dyes under investigation contain a –COOH group to facilitate coupling with biocompatible molecules such as peptides, oligonucleotides, or proteins as well as to highlight the importance of the –COOH group for noncovalent protein labeling and site-selective binding with carrier proteins such as BSA or HSA. Symmetrical dyes containing multiple –COOH groups introduce a complexity in the conjugation process with specific peptides, leading to side reactions and a subsequent decrease in the yield. This complication also contributes to intricate synthetic procedures. On the other hand, unsymmetrical dyes with a single –COOH group can streamline the synthesis of dye conjugates, facilitating a more simple and straightforward process. All the dyes are based on benzo[e]-indole moieties on either side of the squaric acid core. SQ-212 contains a long *N*-substituted dodecyl alkyl group on one-half of the dye, whereas SQ-215 contains a short *N*-substituted ethyl group. The other half anchors the *N*-substituted –COOH group for dyes SQ-212 and SQ-215. SQ-27 bears direct functionalization of the –COOH group on the benzo[e]indole ring. This study then explores the interaction of these dyes with BSA as a model protein in phosphate buffer to investigate the dye's suitability for biosensing and bioimaging applications. The influence and effect of varying alkyl chain lengths and positions of the –COOH group on the interactions with bovine serum albumin (BSA) as a model protein were then followed by *in vitro* and *in vivo* studies involving SQ-212 and SQ-215 with both showing promising capabilities as bioimaging probes. A stable and reproducible signal was obtained from injecting the compounds in white fur-bearing laboratory mice with clear tracking of the dyes until the removal from the organism was possible. Thus, this indicates the efficiency and applicability of dyes and their possible conjugates for *in vivo* imaging techniques.

## 2. EXPERIMENTAL SECTION

**2.1. Materials and Methods.** All of the chemicals used for synthesis were procured from TCI chemicals and Sigma-Aldrich. The dyes and the dye intermediates were analyzed by FAB–mass spectroscopy in the positive-ion monitoring mode followed by high-resolution mass spectroscopy (HRMS). Nuclear magnetic resonance

Scheme 1. Synthesis of Unsymmetrical Squaraine Dyes SQ-212, SQ-215, and SQ-218



(NMR) spectra for structural elucidations were recorded on a JEOL JNM A500 MHz spectrometer in  $\text{CDCl}_3$  solvent with TMS as the internal reference. Solution-state electronic absorption studies were carried out using a JASCO V-530 UV/vis/IR spectrophotometer, while the fluorescence emission spectra were recorded using a JASCO FP-6600 spectrophotometer. For emission studies, the excitation wavelength was 610 nm for all experiments. The excitation (B) and emission (W) bandwidths were kept at 5 and 2 for all studies.

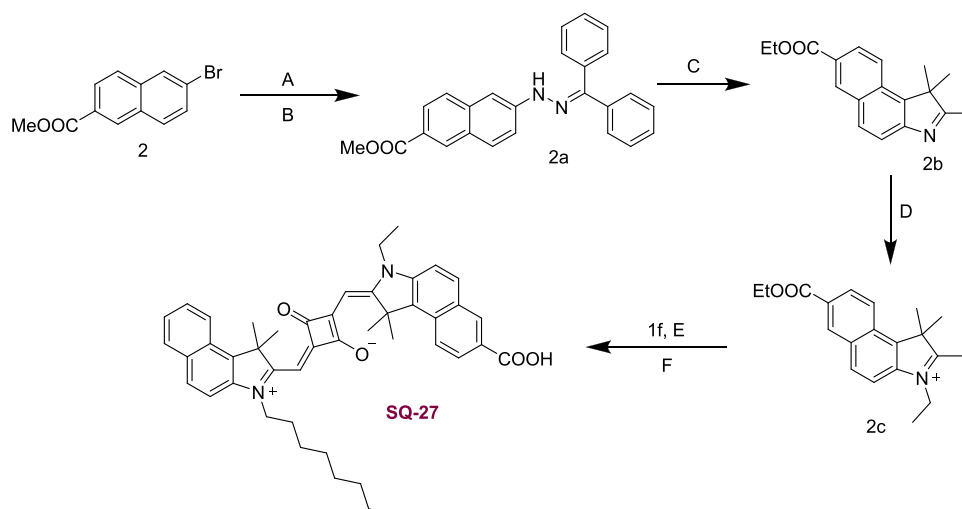
**2.2. Fluorescence Quantum Yield.** The fluorescence quantum yield ( $\phi$ ) of the dyes was calculated by the comparative method<sup>35</sup> with rhodamine 6G as the standard using the following equation.

$$Q = Q_R \left[ \frac{\text{grad}}{\text{grad}_R} \right] \left[ \frac{\eta^2}{\eta_R^2} \right] \quad (1)$$

$Q_R$  represents the quantum yield of the reference or known sample, "grad" signifies the gradient derived from the plot illustrating the integrated fluorescence intensity against the corresponding absorbance,  $\eta$  stands for the refractive index of the solvent, and "grad<sub>R</sub>" denotes the gradient determined for the reference sample. Different

concentrations of the dyes and rhodamine 6G were prepared in  $\text{CHCl}_3$  with the maximum absorption intensity not crossing 0.3. The values of  $Q_R$  for rhodamine 6G (0.95)<sup>36</sup> and  $\eta$  for  $\text{CHCl}_3$  (1.44)<sup>37</sup> were taken from the literature. The emission spectra were obtained by utilizing the absorption spectra's respective absorption maximum ( $\lambda_{\text{max}}$ ) as the excitation wavelength. Subsequently, the integrated fluorescence intensity, which is represented as the area under the emission peak, was measured. A graph correlating the integrated fluorescence intensity with the corresponding absorbance was constructed to determine the gradient.

**2.3. Preparation of Stock Solutions and Study of the Dye–BSA Interaction.** One-millimolar stock solutions (1 mM) of the dyes were prepared in DMSO and  $\text{CHCl}_3$  and diluted to the required concentration when required. Since the dyes were not soluble in PB, the 1 mM DMSO stock solution was diluted to working concentrations of 10 and 2  $\mu\text{M}$  in PB. The dye solutions in PB were stable for more than a week. A 100  $\mu\text{M}$  stock solution of BSA was prepared in 0.1 M phosphate buffer (pH = 7.4). For the dye–BSA interactions, the working volume of the final solution was 5 mL in which the dye's concentration was kept constant at 2  $\mu\text{M}$  while

Scheme 2. Synthesis of Unsymmetrical Squaraine Dye SQ-27<sup>a</sup>

<sup>a</sup>(A) Benzophenone hydrazone, Pd(OAc)<sub>2</sub>, S-BINAP, toluene, RT, and N<sub>2</sub> atmosphere. (B) Sodium *tert*-butoxide, 80 °C. (C) Methyl-isopropyl ketone, PTSA, EtOH, reflux, 18 h. (D) Iodoethane, acetonitrile, reflux, 24 h. (E) Toluene:butanol 1:1, reflux, 18–24 h. (F) 10% NaOH, ethanol, reflux, 30 min.

varying the BSA concentration from 100 nM to 50 μM. The dye–BSA solution was incubated at room temperature for 1 h with continuous stirring before recording the respective absorption and emission spectra. The binding constants ( $K_b$ ) were calculated from previously reported procedures<sup>38</sup> to study the extent of the dye–BSA interaction.

**2.4. Synthesis of Squaraine Dyes and Dye Intermediates.** The squaraine dyes SQ-212, SQ-215, and SQ-218 were synthesized according to Scheme 1, and SQ-27 was synthesized in combination with Schemes 1 and 2. For detailed synthetic procedures and spectral data, see the Supporting Information.

**2.5. Fluorescence of Squaraine Dyes upon an Interaction with Biological Molecules.** Fluorescent dyes were diluted to a final concentration of 10 μM in either H<sub>2</sub>O or phosphate-buffered saline (PBS) with 1% DMSO. A 200 μL solution containing the biologically active substance was prepared in 96-well black plates containing 1% bovine serum albumin (BSA), 10<sup>7</sup> cells/well of Nemeth-Kellner lymphoma cells (NK/Ly), and ascites fluid in separate wells. NK/Ly cells were grown as a liquid tumor in ascites fluid. The ascites was isolated from the peritoneal cavity of mice with a syringe. This cellular suspension was then centrifuged at 1500g to separate the cells and acellular supernatant, which was referred to as ascites fluid.<sup>39</sup> After sedimentation, the cells were washed twice in PBS and used for analysis, while the ascites fluid was dissolved to 50% v/v in PBS due to the technical need for equalizing the volume in all samples. Additionally, some wells were supplemented with a protease inhibitor cocktail at a final concentration of 0.5% (Sigma-Aldrich P8340). This mixture consists of distinct components, namely, AEBSF at a concentration of 104 mM, aprotinin at 80 μM, bestatin at 4 mM, E-64 at 1.4 mM, leupeptin at 2 mM, and pepstatin A at 1.5 mM. Then, squaraine dyes were added to each well to reach a final concentration of 10 μM, and their fluorescence was studied using PerkinElmer BioAssay reader HST7000 at an excitation of 680/10 nm and emission of 720/20 nm and an excitation of 780/10 nm and emission of 820/20 nm.

**2.6. Fluorescent Microscopy.** Fluorescent microscopy was performed as described<sup>40</sup> with an Olympus BX51 fluorescent microscope (Olympus, Tokyo, Japan) equipped with an Omega Filters XF407 filter set with excitation at 630/30 nm and emission at 710/80 nm (Omega Filters, Brattleboro, USA) and a cooled Sony IMX585 sensor-based camera for NIR imaging. Both 40× 0.75 NA, 90× 1.0 NA water immersion, and 100× 1.4 NA oil immersion objectives were used for live-cell imaging. Native Olympus software was used for image processing. Alternatively, a Keyence BZ-X800 fluorescent microscope was used with an appropriate Cy5 fluorescent

filter. For image analysis and quantifications, ImageJ software, developed by the National Institutes of Health in Bethesda, MD, USA, was employed. All image analysis tasks were executed using consistent parameters, which included fixed settings for exposure and compensation.

**2.7. Study of Cell Permeability of Squaraine Dyes.** NK/Ly cells grown in ascites fluid were centrifuged at 1000g to separate the ascites fluid followed by suspending the cells in Hanks' balanced salt solution (HBSS). Squaraine dyes were added to this solution to a final concentration of 50 nM and incubated at 37 °C during the indicated time then put on a slide, covered with a coverslip, and imaged. Imaging of squaraine dyes was done using fluorescent channels suitable for Cy5.

**2.8. Application of Squaraine Dyes for in Vivo Imaging.** White laboratory mice of the Balb/c line of 12 weeks old and weighing 20–25 g were used. Animals were anesthetized and injected intraperitoneally (IP) with 10 μM squaraine dye in H<sub>2</sub>O (containing 1% DMSO) per mouse. Animals were immediately imaged using a LiCor Pearl Trilogy fluorescence analyzer using excitation with a 685 nm laser and emission at a 700 nm channel. The animal studies were approved by the local ethical committee of Danylo Halytsky Lviv National Medical University (permission no. 20201221/P9) and conducted according to the guidelines of the Federation of European Laboratory Animal Science Associations (FELASA).

### 3. RESULTS AND DISCUSSION

**3.1. Photophysical Characterization.** After their successful synthesis, purification, and characterization, the new squaraine dyes were subjected to photophysical investigation using electronic absorption and emission spectroscopies in chloroform, DMSO solvents, and phosphate buffer (pH = 7.4). The optical characterization results are summarized in Tables 1 (in CHCl<sub>3</sub>) and 2 (in DMSO and phosphate buffer). Figure 2 shows the absorption and emission spectra of the dyes in a chloroform solvent. From Table 1, it is evident that varying the alkyl chain length and position of –COOH has a minimal effect on the  $\lambda_{max}$ . All the dyes show sharp and intense light absorption between the 666 and 672 nm wavelength region. The dyes also show a very high molar extinction coefficient, ranging from  $1.7 \times 10^5 \text{ dm}^3 \text{ mol}^{-1} \text{ cm}^{-1}$  to  $2.52 \times 10^5 \text{ dm}^3 \text{ mol}^{-1} \text{ cm}^{-1}$  with the highest for SQ-215. The excitation wavelength was slightly below the corresponding  $\lambda_{max}$  of the

**Table 1. Optical Parameters for Squaraine Dyes in 10  $\mu\text{M}$   $\text{CHCl}_3$  Solution**

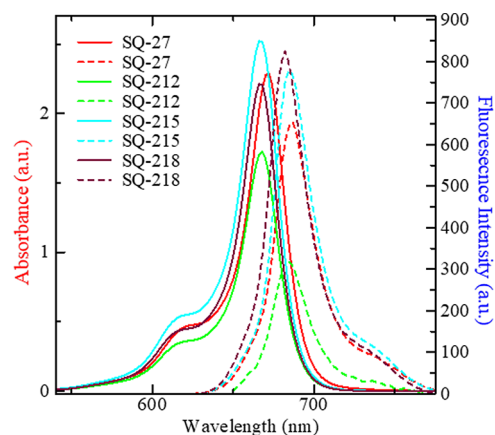
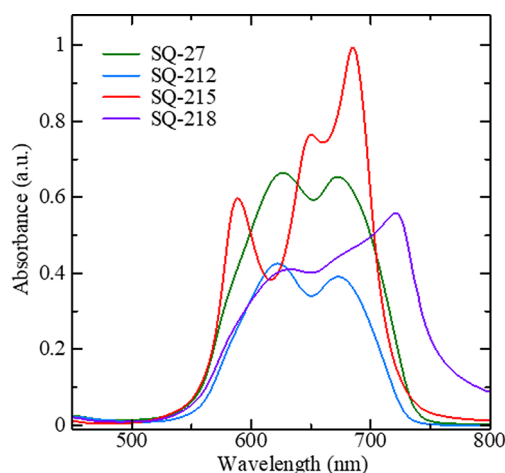
dye	$\lambda_{\text{max}}$ (Abs) (nm)	$\lambda_{\text{max}}$ (Emi) (nm)	Stokes shift (nm)	molar extinction coefficient ( $\epsilon$ ) $\times 10^5$ $\text{dm}^3 \text{mol}^{-1} \text{cm}^{-1}$	quantum yield ( $\phi$ )
SQ-27	672	688	16	2.28	0.12
SQ-212	668	684	16	1.72	0.14
SQ-215	666	686	20	2.52	0.16
SQ-218	666	682	16	2.21	0.16

absorption spectrum at 610 nm. The dyes exhibited an emission peak between the 680 and 690 nm wavelength region with a small Stokes shift of 16–20 nm. This sharp and intense light absorption of squaraine dyes is associated with  $\pi \rightarrow \pi^*$  electronic transitions. A small value of the observed Stokes shift depicts the rigidity of the molecules and the lack of conformational changes after the photoexcitation.

One of the most critical parameters in developing fluorescent probes is the fluorescence quantum yield ( $\phi$ ), which is defined as the ratio of absorbed photons to emitted photons.<sup>41</sup> The product of the  $\phi$  and  $\epsilon$  determines the brightness of the fluorophore, that is, in other words, the strength of the fluorescence signal. As indicated by Table 1, in chloroform, these dyes exhibit in the range of 0.12–0.16, which is typical of squaraine dyes.

Optical parameters deduced from electronic absorption and fluorescence emission spectral investigations for the dyes in DMSO and phosphate buffer are summarized in Table 2. In DMSO, all the dyes show sharp and intense light absorption between the 674 and 680 nm wavelength region with a very high molar extinction coefficient. The dyes exhibited similar behavior with an emission peak between the 692 and 696 nm wavelength region with a small Stokes shift of 16–20 nm. Compared to chloroform, the dyes in DMSO exhibited a red shift of approximately 8–10 nm in the absorption and emission spectra. To investigate the interactions between dyes and biomolecules for biosensing applications, phosphate buffer (PB) solution, pH = 7.4, is most commonly used as it mimics the physiological conditions. Hence, the electronic absorption spectra were measured in 0.1 M PB solution (pH 7.4), as shown in Figure 3. Apart from the primary  $\pi \rightarrow \pi^*$  transition, squaraine dyes also exhibit a vibronic shoulder in chloroform that becomes more prominent, developing into a prominent peak, which has been reported to be an indicator of molecular aggregation. Aggregation in squaraine and cyanine dyes is well-known due to their flat molecular structures.<sup>42,43</sup> A higher absorbance ratio for the vibronic shoulder against the main monomeric dye peak indicates enhanced dye aggregation.<sup>44</sup>

A perusal of Figure 3 reveals that the vibronic shoulder bands in PB get highly pronounced compared to those observed in  $\text{CHCl}_3$  or DMSO solutions, which is indicative of the formation of dye aggregates in PB. Squaraine dyes can form

**Figure 2.** Electronic absorption (solid line) and fluorescence emission (dashed line) spectra of the squaraine dyes in  $\text{CHCl}_3$  (10  $\mu\text{M}$ ).**Figure 3.** Electronic absorption spectra of squaraine dyes (10  $\mu\text{M}$ ) in 0.1 M PB.

aggregates through noncovalent interactions, such as  $\pi$ – $\pi$  stacking, hydrophobic or hydrophilic interactions, van der Waals forces, electrostatic forces, and hydrogen bonding.<sup>45,46</sup> Generally, two types of aggregates, namely, bathochromically shifted J-aggregates and hypsochromically shifted H-aggregates, are reported in squaraine dyes.<sup>47</sup> H-aggregates are primarily characterized by a blue-shifted peak and large Stokes shift compared to the monomer/main peak, while the J-aggregates are characterized by a narrow red-shifted peak with a small Stokes shift.<sup>48–50</sup> The increased dye aggregation in PB is greatly enhanced due to the conducive environment provided by the water to form hydrogen bonds between the dye and water molecules.<sup>51</sup> The presence of the  $-\text{COOH}$  functional group on dyes SQ-27, SQ-212, and SQ-215 further promotes dye aggregation, which can be confirmed from the

**Table 2. Optical Parameters of Squaraine Dyes in DMSO (10  $\mu\text{M}$ ) and PB (10  $\mu\text{M}$ )**

dyes	DMSO				phosphate buffer $\lambda_{\text{max}}$ (Abs) (nm)	
	$\lambda_{\text{max}}$ (Abs) (nm)	$\lambda_{\text{max}}$ (Emi) (nm)	Stokes's shift (nm)	molar extinction coefficient ( $\epsilon$ ) $\times 10^5$ $\text{dm}^{-3} \text{mol}^{-1} \text{cm}^{-1}$	main Peak	shoulder peak(s)
SQ-27	680	696	16	2.47	674	626
SQ-212	676	692	16	1.71	674	622
SQ-215	674	694	20	2.44	650	588, 686
SQ-218	674	692	18	2.24	676	632, 720

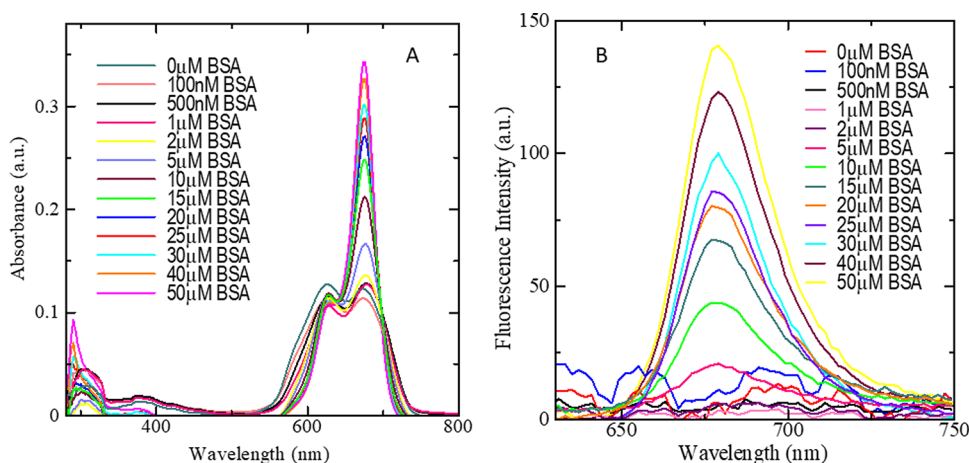


**Figure 4.** Absorption (A) and emission spectral (B) changes for dye SQ-27 (2  $\mu\text{M}$ ) upon interacting with the varying concentrations of BSA.

spectra of SQ-218, which lacks a  $-\text{COOH}$  group, and the main peak's intensity is relatively higher than the shoulder peak (Figure 3). The carboxylic acid group tends to act as both a hydrogen bond acceptor and donor.<sup>52</sup> Therefore, the presence of the  $-\text{COOH}$  group in the molecular framework can significantly increase the chances of hydrogen-bond formation in aqueous media. The chain length also influences the dye aggregate formation in PB. In the case of *N*-ethyl-substituted SQ-215, the formation of both H-aggregates and J-aggregates is seen (Figure 3). The peak of H-aggregates appears around 588 nm, whereas the peak of J-aggregates appears at around 686 nm. In the case of SQ-27 and SQ-212, only H-aggregate formation is seen with the main peak above 670 nm and the shoulder peak around 620 nm. This is due to the long alkyl chain substitution (octyl and dodecyl), which reduces the formation of aggregates due to steric hindrances. Long alkyl chains also increase the lipophilicity of the dye molecules, thereby slightly decreasing the extent of aggregate formation due to the hydrophobic effect.<sup>53</sup> SQ-218 containing both ethyl and dodecyl chains shows the presence of both the aggregates. However, the shoulder and main peak are red-shifted compared to other dyes. The peak corresponding to H-aggregates and J-aggregates appears at 632 and 720 nm, respectively. The small hump observed at 676 nm corresponds to the main peak. Thus, long alkyl chains in the molecular framework prevent J-aggregate formation, promoting only the formation of H-aggregates, which can be exploited to control the aggregates' formation behavior selectively. Fluorescence emission spectra showed complete quenching of the fluorescence for all the dyes in PB. Thus, these dyes are ideal and promising probes for fluorescence on/off and FRET-based biosensing applications. This is advantageous because the probes can be tailored to enhance the fluorescence signal upon adding the analyte of interest, such as biomolecules of clinical significance. Thus, under physiological conditions, they stay in the fluorescent-off state and fluorescent-on state upon the interaction of the analyte. To further validate this, the interaction of these dyes with BSA as a model protein was studied in PB.

**3.2. Interaction of Dyes with BSA.** Labeling biomolecules with fluorescent probes by noncovalent methods is preferred in biosensing and bioimaging applications because it avoids the complications of a chemical reaction and purification steps and provides quick response times.<sup>28</sup> In this regard, human serum albumin (HSA)/BSA has been used

as a model protein to study the interaction of probes with proteins. Patonay and co-workers first studied the noncovalent labeling of NIR dyes with HSA.<sup>54</sup> Due to its high homology with HSA in the amino acid sequences, BSA has prominently been used as a model protein to investigate the interactions between dye and protein.<sup>55,56</sup> It can be seen from Figure 4 that, with the increasing concentrations of BSA, a decrease in the intensity of the SQ-27's shoulder peak and an increase in the intensity of the main peak at 674 nm are observed, indicating the prevention of dye aggregation due to dye–BSA interactions. At the same time, this enhanced dye–BSA interaction led to the reappearance of a fluorescence signal at 678 nm with a tremendous increase with increasing concentrations of BSA.

Long alkyl chain (dodecyl)-substituted dye SQ-212 also followed a similar trend of decrease in dye aggregation with a concomitant increase in the fluorescence intensity with an increasing concentration of BSA, which is shown in Figure 5,

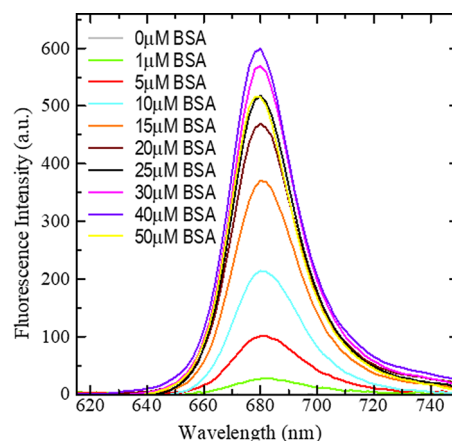


**Figure 5.** Changes in the fluorescence spectra of dye SQ-212 as a function of varying concentrations of BSA.

but with a differential enhancement in the fluorescence intensities upon their interaction with BSA. SQ-212 demonstrated nearly two times of enhanced fluorescence compared to dye SQ-27. This could be associated with their different structural features, leading to differential interactions with BSA. It can be seen from Figure 1 that SQ-27 contains  $-\text{COOH}$  directly substituted in the main aromatic ring, while SQ-212

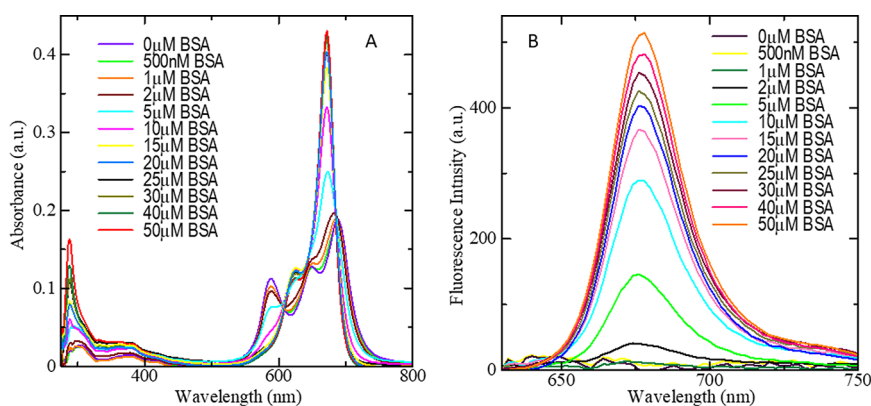


**Figure 6.** Absorption (A) and emission spectra (B) of SQ-215 ( $2\ \mu\text{M}$ ) with varying concentrations of BSA.

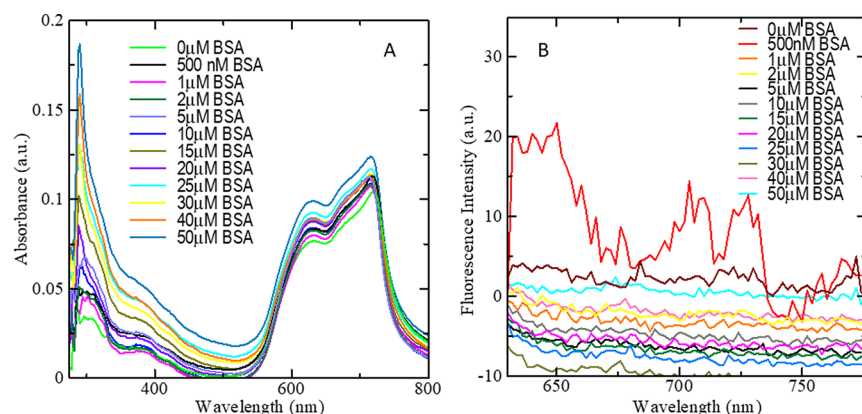


**Figure 7.** Absorption (A) and emission spectra (B) of SQ-218 ( $2\ \mu\text{M}$ ) with varying concentrations of BSA.

contains the  $-\text{COOH}$  group substituted in the *N*-alkyl side chain with different spacer lengths, which will be discussed later by structure–property correlations. Investigation of the concentration-dependent differential changes in the fluorescence intensities for different sensitizers revealed that the dyes SQ-212 and SQ-27 are sensitive to BSA up to 1 and 5  $\mu\text{M}$ , respectively.

To understand the role of the alkyl chain length on the nature of aggregate formation and their impact on interaction with BSA, analogous dye probes of SQ-212 with a short alkyl chain length (ethyl) as SQ-215 were designed and subjected to their optical characterization and interaction with BSA. Figure 6 depicts the absorption and fluorescence spectral changes for dye SQ-215 upon its interaction with different concentrations of BSA. A perusal of this figure corroborates that, with increasing concentrations of BSA, there is an initial and slight blue shift up to 5  $\mu\text{M}$  in the peak rising out of the formation of J-aggregates with little change in the absorption intensities of all three peaks appearing at 588, 650, and 686 nm. After a further increase in the BSA concentration beyond 5  $\mu\text{M}$ , the J-aggregate peak blue-shifts and merges with the main peak with the new peak appearing at 672 nm showing a sharper peak along with the increase in the intensity. On the other hand, the H-aggregate peak at 588 nm red-shifts and becomes insignificant, which is similar to the monomer's absorption. Thus, at BSA concentrations from 5  $\mu\text{M}$  onward, the breaking of H-aggregates and J-aggregates leads to the appearance of the fluorescence signal at 678 nm, whose intensity increases with the BSA concentration. SQ-215 was sensitive to BSA at concentrations of up to 1  $\mu\text{M}$ .

In contrast to the dyes bearing the  $-\text{COOH}$  functional group, the dye–BSA interaction of SQ-218 lacking the  $-\text{COOH}$  group was quite different, as shown in Figure 7. Interestingly, there was no change in the aggregation behavior of SQ-218 in both absorption and emission studies, which is further affirmed by the lack of appearance of any fluorescence signal with increasing concentrations of BSA. This suggests the need and importance of a suitable functional group for noncovalent interactions between the dye molecule and protein. Throughout this study, there was no denaturation of the BSA caused by the dyes as the peak at 280 nm (Figures 4, 6, and 7) attributed to BSA that increases in intensity with the increasing concentrations of BSA confirms this. BSA contains two separate active sites: one being a hydrophobic site labeled as site I and the other a hydrophilic site referred to as site II. The binding interactions of site I are primarily hydrophobic in nature, whereas the binding interactions of site II involve a combination of hydrophobic, hydrogen-bonding, and electrostatic interactions.<sup>57–59</sup>

Observing all the dye's interactions with BSA, it is evident that a  $-\text{COOH}$  group in the dye's structure is essential for them to interact with BSA and break the formation of the aggregates. This is affirmed as the dye SQ-218 lacking the  $-\text{COOH}$  group showed no fluorescence signal or change in the absorption spectra with increasing concentrations of BSA. This indicates that this class of squaraine dyes (with two benzo[e]indole moieties) most probably interacts with site II through hydrophilic interactions with hydrogen bonding as the most probable one. To further investigate this, the dye–BSA conjugate was subjected to ligand displacement studies with

well-known site-specific ligands such as dansylamide (DNSA) for site I and dansylproline (DP) for site II.<sup>60–62</sup>

The addition of varying concentrations of DP to the SQ-215-BSA conjugate resulted in a gradual decrease in the fluorescence intensity (Figure 8), which is due to the

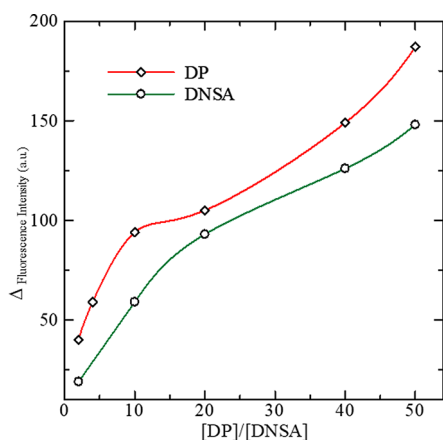


**Figure 8.** Change in the fluorescence intensity with varying concentrations of DP and DNSA to the SQ-215 (2  $\mu$ M)–BSA (50  $\mu$ M) conjugate.

displacement of SQ-215 by DP. Similar results were obtained with DNSA, but the fluorescence intensity decrease was smaller than that for DP (Figure 8). Thus, Figure 8 indicates that these squaraine derivatives preferably bind to site II noncovalently and less effectively at site I.

Dyes with  $-\text{COOH}$  in *N*-alkyl substitution (SQ-212 and SQ-215) showed a more pronounced fluorescence intensity than SQ-27 with  $-\text{COOH}$  directly functionalized to the main ring, which could be attributed to the fact that  $-\text{COOH}$  substituted in the alkyl chain has more freedom of rotation compared to  $-\text{COOH}$  being substituted on the aromatic main ring. Having greater freedom of rotation gives  $-\text{COOH}$  more ability to access the active sites of BSA, thereby increasing the interactions with BSA, which in turn leads to a more effective breaking of the dye aggregates, resulting in an enhanced fluorescence signal.

To further compare the ability of the dye's binding and their relative association with BSA quantitatively, the apparent binding constant ( $K_a$ ) was calculated, as shown in Figure 9. The slope of the plot gave the corresponding value of the

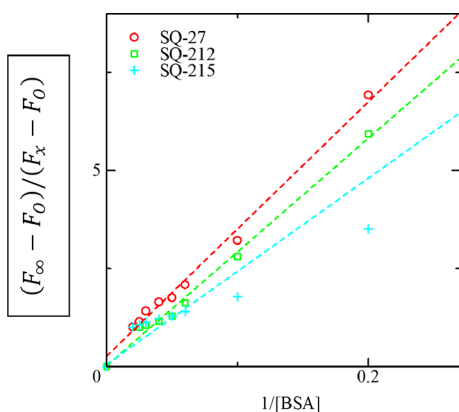


**Figure 9.** Plot of  $(F_\infty - F_0)/(F_x - F_0)$  vs  $[\text{BSA}]^{-1}$  of the dyes (2  $\mu$ M).

binding constant ( $K_a$ ), as summarized in Table 3. It can be seen from this table that the binding constants of the dyes in

**Table 3. Binding Constants for the Dyes with Their Interaction with BSA**

dye	
SQ-27	$3.30 \pm 0.03 \times 10^7/\text{mol}$
SQ-212	$2.11 \pm 0.06 \times 10^7/\text{mol}$
SQ-215	$3.61 \pm 0.11 \times 10^7/\text{mol}$

this study show an order higher in magnitude compared to typical squaraine dyes.<sup>55</sup> SQ-215 showed the highest  $K_a$  among the dyes in this study. Analysis of Job's plot showed that BSA interacts with all the dyes in a 2:1 ratio. The Job's plot for all the dyes is given in the Supporting Information.

### 3.3. Interaction of Dyes with Biological Compounds.

Compounds SQ-212 and SQ-215 were selected as the most promising candidates for further *in vitro* and *in vivo* bioimaging applications. Initially, the squaraine dyes were incubated with various biological compounds, including 1% BSA, 50% ascites fluid (serving as the medium for growth of NK/Ly tumor cells in mice abdomen), and  $10^7$  NK/Ly cells. This incubation was carried out in either PBS or water with the inclusion of a protease inhibitor cocktail to prevent compound degradation and aggregate formation when interacting with cells or ascites. For SQ-212, a time-dependent increase in the fluorescence intensity was observed, reaching a plateau after approximately 30 min. Notably, the highest fluorescence signal was observed when the mixture was interacting with 1% BSA solution. Importantly, protease inhibitors had no discernible effect on the compound's fluorescence as indicated by the signal in the presence of these inhibitors (dotted lines in Figure 10). In the absence of proteins in the mixture (PBS alone or water), the fluorescence of SQ-212 remained at minimally detectable levels. In contrast, SQ-215 exhibited a rapid increase in fluorescence upon an interaction with the components, reaching 10,000 MFI within 10 min, which is 10-fold of SQ-212. As with SQ-212, BSA produced the strongest signal, while solutions lacking proteins showed no detectable fluorescence. Notably, the fluorescence of SQ-215 was nearly five times brighter than that of SQ-212 under the same conditions, owing to a higher quantum yield and molar extinction coefficient of SQ-215.

**3.4. In Vitro studies of SQ-212 and SQ-215.** To assess the ability of the indicated compounds to penetrate cell membranes, vital microscopy of NK/Ly cells was performed. These cells, characterized by their larger diameter, serve as an excellent model for studying the intracellular localization of compounds.<sup>63</sup> At a concentration of 50 nM, SQ-212 did not penetrate the cell membrane but accumulated on the plasma membrane, as shown in Figure 11. This accumulation resulted in a high background signal in the medium surrounding the cells. In contrast, SQ-215 rapidly penetrated the cells, exhibiting localization within the cytoplasm. Although no specific organelle accumulation was observed, some dyes remained in the plasma membrane. As the dye was consumed from the medium, no background signal was detected (Figure 11). Thus, having two similar dyes with one cell-permeant and the other cell-non-permeant provides a wide range of options for various visualization applications.

Differential cell permeabilities can be explained by the change in lipophilicity of SQ-212 and SQ-215 brought out by

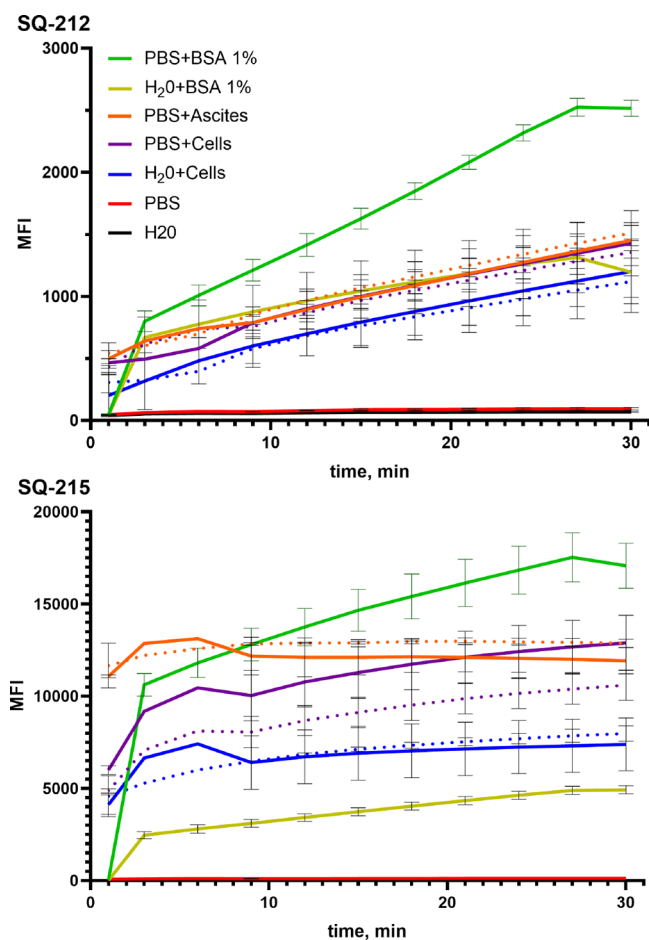


**Figure 10.** Fluorescence of SQ-212 and SQ-215 upon an interaction with biopolymers. Dotted lines indicate the same substance as solid with the addition of a protease inhibitor cocktail.

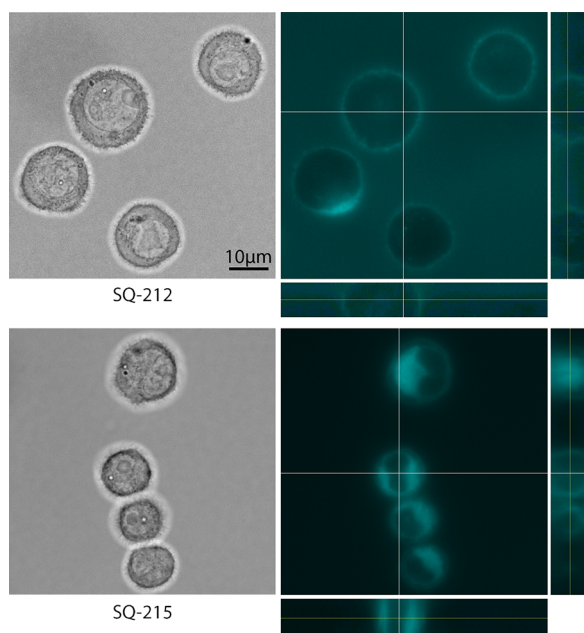


**Figure 11.** Incubation of mammalian cells with SQ-212 and SQ-215 dyes demonstrated different cell permeabilities.

the change in the *N*-alkyl substitution. The cell membrane plays a critical role in maintaining the cellular integrity and

regulating the passage of molecules in and out of the cell. It consists of a phospholipid bilayer with embedded proteins that serve various functions. The lipophilicity or hydrophobicity of a molecule is a key determinant of its cell permeability. Lipophilic molecules characterized by their ability to dissolve in the lipid-rich environment of the cell membrane can readily traverse the membrane via passive diffusion. However, the degree of lipophilicity must be finely balanced, as excessively lipophilic molecules may become trapped within the lipid bilayer, hindering their passage.<sup>64–66</sup> The partition coefficient (*p*) in terms of the log *P* value is a quantitative measure of a molecule's lipophilicity calculated by comparing the distribution of a molecule between a hydrophobic (octanol) and hydrophilic (water) phase. The log *P* value represents the logarithm of the ratio of the concentration of the molecule in the organic phase to its concentration in the aqueous phase. The log *P* value directly influences the cell permeability of molecules. As a general rule, molecules with higher log *P* values (indicating greater lipophilicity) tend to exhibit increased cell permeability. This is because highly lipophilic compounds can efficiently traverse the lipid bilayer of the cell membrane through passive diffusion.<sup>67–69</sup> However, excessively high log *P* values may lead to trapping of the molecule within the bilayer/membrane itself. The log *P* values of SQ-212 and SQ-215 were calculated computationally using the SwissADME tools<sup>70</sup> and were found to be 10.88 and 8.15, respectively. The high log *P* value for SQ-212 is attributed to the long *N*-alkyl substitution (dodecyl). SQ-212, which is characterized by a very high log *P* value of 10.88, accumulates within the plasma membrane and is unable to penetrate into the cell. In contrast, SQ-215, exhibiting a comparatively lower log *P* value of 8.15 in comparison to SQ-212, permeates the plasma membrane, leading to dye localization in the cytoplasm as depicted in Figure 11.

### 3.5. In Vivo studies of SQ-212 and SQ-215.

Transitioning from the preceding *in vitro* studies, the investigation was further extended to *in vivo* imaging, allowing for an examination of the compound's behavior within living organisms. Intraperitoneal injection of 10 μM dye in H<sub>2</sub>O containing 1% DMSO per mouse facilitated precise visualization of the signal distribution within the cell body. Imaging was done using the same setup at indicated time points. Fluorescence was detected at 720 nm and overlaid with a bright field image of the animal. SQ-212 displayed a more uniform distribution, which is likely attributed to its lower cell permeability and distribution through the vascular system, while SQ-215 exhibited a higher concentration near the injection site, as depicted in Figure 12. Importantly, neither toxic effects were observed nor any behavioral changes were detected in mice up to 7 days following the compounds' injection. Figure 12 illustrates the intense fluorescence exhibited by the dyes in tissues, affirming the absence of quenching, degradation by the phagocytic system, or binding with blood components. This accentuates the suitability of SQ-212 and SQ-215 as promising candidates for imaging applications.

Both dyes were excreted through two pathways—urine and stool—following conjugation in the liver, subsequent transfer to bile, and eventual release into the intestine. Validation of this process was conducted through imaging of both stool and the wet bedding within the cage. Notably, the elimination process was more rapid for SQ-215 with discernible accumulation in the liver apparent at approximately 120 min

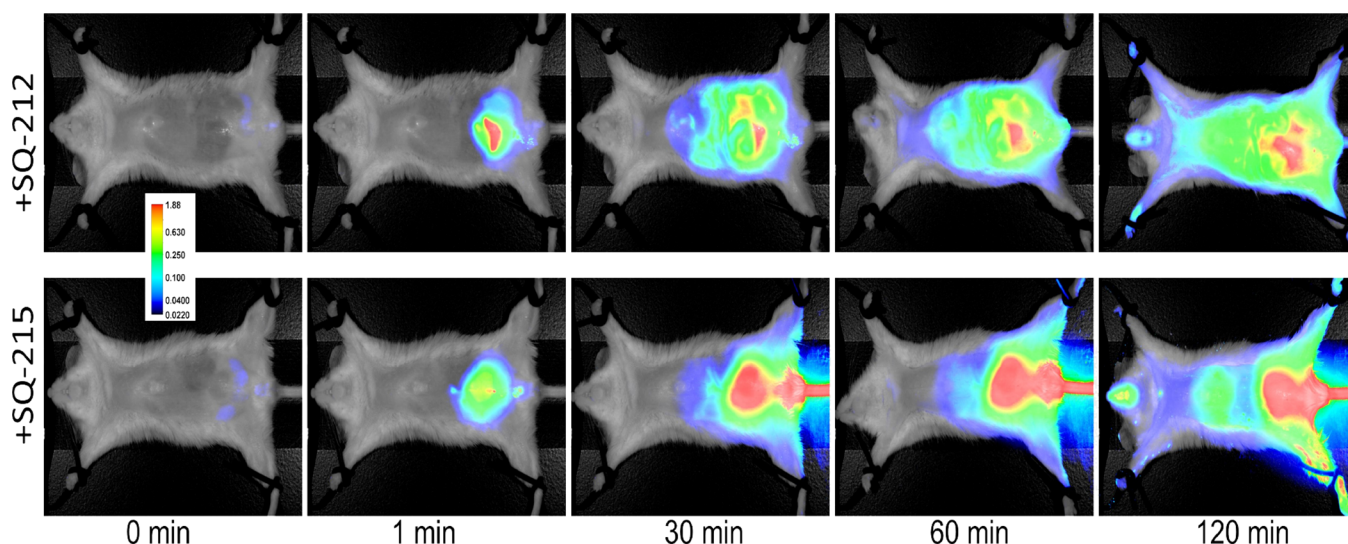


Figure 12. Distribution of SQ-212 and SQ-215 in the body of laboratory mice.

(Figure 12). Conversely, the removal rate for SQ-212 was slower as evidenced by a persistent signal in the liver, intestine, and urinary bladder even after a 24 h period (Figure 13).

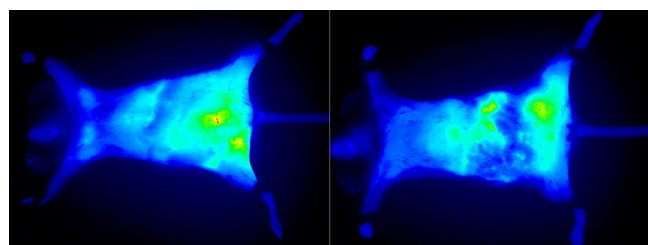


Figure 13. Weak fluorescence signal shown by SQ-212 after 24 h, indicating slower excretion.

#### 4. CONCLUSIONS

Three new unsymmetrical squaraine dyes with  $-\text{COOH}$  functionalization (SQ-27, SQ-212, and SQ-215) and one without  $-\text{COOH}$  functionalization (SQ-218) have been successfully synthesized and characterized. Photophysical characterization followed by dye-BSA interaction studies were conducted to study these dyes' applicability as fluorescent probes for sensing and noncovalent labeling of proteins. All of the dyes showed complete fluorescence quenching in PB owing to dye aggregate formation. Interaction of the carboxy-functionalized dyes (SQ-27, SQ-212, and SQ-215) with BSA indicated the formation of a dye-BSA conjugate, preventing dye aggregation and eventually leading to the enhanced fluorescence signal. SQ-218, lacking the  $-\text{COOH}$  group, showed no fluorescence signal after the addition of BSA, thereby affirming the importance of the  $-\text{COOH}$  group for the noncovalent dye-BSA interactions. Dyes with the  $-\text{COOH}$  group substituted in the *N*-alkyl chain (SQ-212 and SQ-215) showed a higher fluorescence intensity than SQ-27, which has direct ring  $-\text{COOH}$  functionalization. All dyes showed very high binding affinities toward BSA in the order of  $10^7/\text{mol}$ . In vitro investigation revealed distinct and differential behavior by SQ-dyes (SQ-212 and SQ-215), where SQ-212 exhibited no cell penetration, leading to an accumulation on the plasma membrane, whereas SQ-215 showcased rapid cell penetration

and subsequent cytoplasmic localization. Additionally, insights into the distribution of these compounds within living organisms were revealed through in vivo imaging. Both the dyes showed an absence of quenching, no degradation by the phagocytic system, and binding with blood components, leading to a stable and strong fluorescence signal. SQ-212 displayed a more uniform distribution, which is attributed to its lower cell permeability, while SQ-215 concentrated more near the injection site. A noteworthy outcome of this study was the absence of any toxic effects or behavioral changes in mice up to 7 days after compound injections. This nontoxic profile suggests the potential for further development of these dyes for biomedical and imaging applications, while the combination of cell-permeant SQ-215 and cell-nonpermeant SQ-212 dyes presents a versatile tool for a multitude of visualization applications. The dyes can further be coupled with specific probes for selective tissue imaging, sensing the environment around specific tissues, and biomarker detection.

#### ■ ASSOCIATED CONTENT

##### Supporting Information

The Supporting Information is available free of charge at <https://pubs.acs.org/doi/10.1021/acsabm.3c00997>.

Detailed synthetic procedures for dye synthesis, NMR and mass spectroscopy data of the dyes, and Job's plot for dye-BSA interactions (PDF)

#### ■ AUTHOR INFORMATION

##### Corresponding Authors

Rostyslav Bilyy – Lectinotest R&D, 79000 Lviv, Ukraine; Department of Histology, Cytology & Embryology, Danylo Halytsky Lviv National Medical University, 79010 Lviv, Ukraine; [orcid.org/0000-0002-2344-1349](https://orcid.org/0000-0002-2344-1349); Email: [r.bilyy@gmail.com](mailto:r.bilyy@gmail.com)

Shyam S. Pandey – Graduate School of Life Science and System Engineering, Kyushu Institute of Technology, 808-0196 Kitakyushu, Japan; [orcid.org/0000-0001-8102-1003](https://orcid.org/0000-0001-8102-1003); Email: [shyam@life.kyutech.ac.jp](mailto:shyam@life.kyutech.ac.jp)

## Authors

Sai Kiran Mavileti – Graduate School of Life Science and System Engineering, Kyushu Institute of Technology, 808-0196 Kitakyushu, Japan

Galyna Bila – Lectinotest R&D, 79000 Lviv, Ukraine; Department of Histology, Cytology & Embryology, Danylo Halytsky Lviv National Medical University, 79010 Lviv, Ukraine; [orcid.org/0000-0002-8084-8268](https://orcid.org/0000-0002-8084-8268)

Valentyn Utko – Lectinotest R&D, 79000 Lviv, Ukraine

Evgenia Bila – Lectinotest R&D, 79000 Lviv, Ukraine; Department of Organic Chemistry, Ivan Franko National University of Lviv, 79005 Lviv, Ukraine

Tamaki Kato – Graduate School of Life Science and System Engineering, Kyushu Institute of Technology, 808-0196 Kitakyushu, Japan

Complete contact information is available at:  
<https://pubs.acs.org/10.1021/acsabm.3c00997>

## Author Contributions

S.K.M. and G.B. contributed in the conceptualization, investigation, resources, data curation, and writing—original draft preparation. V.U., E.B., and T.K. contributed in resources and writing—original draft preparation. R.B. and S.S.P. contributed in conceptualization, validation, investigation, resources, writing (review and editing), supervision, and project administration.

## Funding

This work has not in any way earned research funding or grants from any commercial, agencies, or nonprofit organizations.

## Notes

The authors declare no competing financial interest.

## ACKNOWLEDGMENTS

S.K.M. and S.S.P. thanks the Ministry of Education, Culture, Sports, Science and Technology (MEXT), Govt. of Japan. This work was financially supported by the European Union's Horizon 2020 research and innovation program under grant agreement no. 872331 NoBiasFluors (Nonbiased Fluorescent Dyes as Markers of Drugs for Optical in Cellular and in Vivo Imaging" and Simons Foundation grant no. 1037973 to E.B. In vivo imaging facilities used in the current research were established under a grant of National Research Foundation of Ukraine no. 2020.02/0131.

## REFERENCES

- (1) Thomas, J. A. Optical Imaging Probes for Biomolecules: An Introductory Perspective. *Chem. Soc. Rev.* **2015**, *44* (14), 4494–4500.
- (2) Rudin, M.; Weissleder, R. Molecular Imaging in Drug Discovery and Development. *Nat. Rev. Drug Discovery* **2003**, *2* (2), 123–131.
- (3) Brancato, R.; Trabucchi, G. Fluorescein and Indocyanine Green Angiography in Vascular Chorioretinal Diseases. *Semin. Ophthalmol.* **1998**, *13* (4), 189–198.
- (4) Flower, R. W.; Hochheimer, B. F. Indocyanine Green Dye Fluorescence and Infrared Absorption Choroidal Angiography Performed Simultaneously with Fluorescein Angiography. *Johns Hopkins Med. J.* **1976**, *138* (2), 33–42.
- (5) Lavis, L. D.; Raines, R. T. Bright Ideas for Chemical Biology. *ACS Chem. Biol.* **2008**, *3* (3), 142–155.
- (6) Fabian, J.; Nakazumi, H.; Matsuoka, M. Near-Infrared Absorbing Dyes. *Chem. Rev.* **1992**, *92* (6), 1197–1226.

(7) Wang, L.; Li, L.; Fan, Y.; Wang, H. Host-Guest Supramolecular Nanosystems for Cancer Diagnostics and Therapeutics. *Adv. Mater.* **2013**, *25* (28), 3888–3898.

(8) Tan, X.; Luo, S.; Wang, D.; Su, Y.; Cheng, T.; Shi, C. A NIR Heptamethine Dye with Intrinsic Cancer Targeting, Imaging and Photosensitizing Properties. *Biomaterials* **2012**, *33* (7), 2230–2239.

(9) Licha, K.; Welker, P.; Weinhart, M.; Wegner, N.; Kern, S.; Reichert, S.; Gemeinhardt, I.; Weissbach, C.; Ebert, B.; Haag, R.; Schirner, M. Fluorescence Imaging with Multifunctional Polyglycerol Sulfates: Novel Polymeric near-IR Probes Targeting Inflammation. *Bioconjugate Chem.* **2011**, *22* (12), 2453–2460.

(10) Weissleder, R. A Clearer Vision for in Vivo Imaging. *Nat. Biotechnol.* **2001**, *19* (4), 316–317.

(11) Terpetschnig, E.; Wolfbeis, O. S. Luminescent Probes for NIR Sensing Applications. In *Near-Infrared Dyes for High Technology Applications*; Springer: Dordrecht, 1998; pp 161–182. DOI: [10.1007/978-94-011-5102-3\\_8](https://doi.org/10.1007/978-94-011-5102-3_8).

(12) Yuan, L.; Lin, W.; Zhao, S.; Gao, W.; Chen, B.; He, L.; Zhu, S. A Unique Approach to Development of Near-Infrared Fluorescent Sensors for in Vivo Imaging. *J. Am. Chem. Soc.* **2012**, *134* (32), 13510–13523.

(13) Kosaka, N.; Ogawa, M.; Choyke, P. L.; Kobayashi, H. Clinical Implications of Near-Infrared Fluorescence Imaging in Cancer. *Futur. Oncol.* **2009**, *5* (9), 1501–1511.

(14) Kaibori, M.; Kosaka, H.; Matsui, K.; Ishizaki, M.; Matsushima, H.; Tsuda, T.; Hishikawa, H.; Okumura, T.; Sekimoto, M. Near-Infrared Fluorescence Imaging and Photodynamic Therapy for Liver Tumors. *Front. Oncol.* **2021**, *11*, No. 638327, DOI: [10.3389/fonc.2021.638327](https://doi.org/10.3389/fonc.2021.638327).

(15) Owens, E. A.; Henary, M.; El Fakhri, G.; Choi, H. S. Tissue-Specific Near-Infrared Fluorescence Imaging. *Acc. Chem. Res.* **2016**, *49* (9), 1731–1740.

(16) Ji, Y.; Jones, C.; Baek, Y.; Park, G. K.; Kashiwagi, S.; Choi, H. S. Near-Infrared Fluorescence Imaging in Immunotherapy. *Adv. Drug Delivery Rev.* **2020**, *167*, 121–134.

(17) Keil, D. Synthesis and Characterization of 1,3-Bis-(2-Dialkylamino-5-Thienyl)-Substituted Squaraines 128; 148; a Novel Class of Intensively Coloured Panchromatic Dyes. *Dye. Pigment.* **1991**, *17* (1), 19–27.

(18) Sreejith, S.; Carol, P.; Chithra, P.; Ajayaghosh, A. Squaraine Dyes: A Mine of Molecular Materials. *J. Mater. Chem.* **2008**, *18* (3), 264–274.

(19) Law, K. Y. Squaraine Chemistry. Design, Synthesis and Xerographic Properties of a Highly Sensitive Unsymmetrical Fluorinated Squaraine. *Chem. Mater.* **1992**, *4* (3), 605–611.

(20) Ilina, K.; MacCuaig, W. M.; Laramie, M.; Jeouty, J. N.; McNally, L. R.; Henary, M. Squaraine Dyes: Molecular Design for Different Applications and Remaining Challenges. *Bioconjugate Chem.* **2020**, *31* (2), 194–213.

(21) Markova, L. I.; Terpetschnig, E. A.; Patsenker, L. D. Comparison of a Series of Hydrophilic Squaraine and Cyanine Dyes for Use as Biological Labels. *Dye. Pigment.* **2013**, *99* (3), 561–570.

(22) Hu, L.; Yan, Z.; Xu, H. Advances in Synthesis and Application of Near-Infrared Absorbing Squaraine Dyes. *RSC Adv.* **2013**, *3* (21), 7667.

(23) Ahn, H.-Y.; Yao, S.; Wang, X.; Belfield, K. D. Near-Infrared-Emitting Squaraine Dyes with High 2PA Cross-Sections for Multiphoton Fluorescence Imaging. *ACS Appl. Mater. Interfaces* **2012**, *4* (6), 2847–2854.

(24) McEwen, J. J.; Wallace, K. J. Squaraine Dyes in Molecular Recognition and Self-Assembly. *Chem. Commun.* **2009**, *42*, 6339.

(25) Ros-Lis, J. V.; Garcia, B.; Jiménez, D.; Martínez-Máñez, R.; Sancenón, F.; Soto, J.; Gonzalvo, F.; Valldecabres, M. C. Squaraines as Fluoro-Chromogenic Probes for Thiol-Containing Compounds and Their Application to the Detection of Biorelevant Thiols. *J. Am. Chem. Soc.* **2004**, *126* (13), 4064–4065.

(26) Kolev, T. M.; Yancheva, D. Y.; Stoyanov, S. I. Synthesis and Spectral and Structural Elucidation of Some Pyridinium Betaines of

Squaric Acid: Potential Materials for Nonlinear Optical Applications. *Adv. Funct. Mater.* **2004**, *14* (8), 799–805.

(27) Escobedo, J. O.; Rusin, O.; Lim, S.; Strongin, R. M. NIR Dyes for Bioimaging Applications. *Curr. Opin. Chem. Biol.* **2010**, *14* (1), 64–70.

(28) Patonay, G.; Salon, J.; Sowell, J.; Strekowski, L. Noncovalent Labeling of Biomolecules with Red and Near-Infrared Dyes. *Molecules* **2004**, *9* (3), 40–49.

(29) Oswald, B.; Patsenker, L.; Duschl, J.; Szmackinski, H.; Wolfbeis, O. S.; Terpetschnig, E. Synthesis, Spectral Properties, and Detection Limits of Reactive Squaraine Dyes, a New Class of Diode Laser Compatible Fluorescent Protein Labels. *Bioconjugate Chem.* **1999**, *10* (6), 925–931.

(30) Johnson, J. R.; Fu, N.; Arunkumar, E.; Leevy, W. M.; Gammon, S. T.; Piwnica-Worms, D.; Smith, B. D. Squaraine Rotaxanes: Superior Substitutes for Cy-5 in Molecular Probes for Near-Infrared Fluorescence Cell Imaging. *Angew. Chem.* **2007**, *119* (29), 5624–5627.

(31) Gassensmith, J. J.; Arunkumar, E.; Barr, L.; Baumes, J. M.; DiVittorio, K. M.; Johnson, J. R.; Noll, B. C.; Smith, B. D. Self-Assembly of Fluorescent Inclusion Complexes in Competitive Media Including the Interior of Living Cells. *J. Am. Chem. Soc.* **2007**, *129* (48), 15054–15059.

(32) Gao, F.-P.; Lin, Y.-X.; Li, L.-L.; Liu, Y.; Mayerhöffer, U.; Spent, P.; Su, J.-G.; Li, J.-Y.; Würthner, F.; Wang, H. Supramolecular Adducts of Squaraine and Protein for Noninvasive Tumor Imaging and Photothermal Therapy in Vivo. *Biomaterials* **2014**, *35* (3), 1004–1014.

(33) Volkova, K. D.; Kovalska, V. B.; Tatarski, A. L.; Patsenker, L. D.; Kryvorotenko, D. V.; Yarmoluk, S. M. Spectroscopic Study of Squaraines as Protein-Sensitive Fluorescent Dyes. *Dye. Pigment.* **2007**, *72* (3), 285–292.

(34) Barbero, N.; Butnarusu, C.; Visentin, S.; Barolo, C. Squaraine Dyes: Interaction with Bovine Serum Albumin to Investigate Supramolecular Adducts with Aggregation-Induced Emission (AIE) Properties. *Chem. - Asian J.* **2019**, *14* (6), 896–903.

(35) Brandner, B. Implementation of a Comparative Method for Measuring Photoluminescence Quantum Yield of Novel Compounds in Solution. Undergraduate Thesis; Oregon State University, 2016, 6–7.

(36) Kubin, R. F.; Fletcher, A. N. Fluorescence Quantum Yields of Some Rhodamine Dyes. *J. Lumin.* **1982**, *27* (4), 455–462.

(37) Asfour, A. F. A.; Dullien, F. A. L. Viscosities and Densities of Four Binary Liquid Systems at 25.00 Degree C. *J. Chem. Eng. Data* **1981**, *26* (3), 312–316.

(38) Saikiran, M.; Sato, D.; Pandey, S. S.; Ohta, T.; Hayase, S.; Kato, T. Photophysical Characterization and BSA Interaction of the Direct Ring Carboxy Functionalized Unsymmetrical NIR Cyanine Dyes. *Dye. Pigment.* **2017**, *140*, 6–13.

(39) Özkan, H. G.; Thakor, V.; Xu, H.-G.; Bila, G.; Bilyy, R.; Bida, D.; Böttcher, M.; Mouggiakakos, D.; Tietze, R.; Mokhir, A. Anticancer Aminoferrrocene Derivatives Inducing Production of Mitochondrial Reactive Oxygen Species. *Chem. - Eur. J.* **2022**, *28* (30), No. e202104420, DOI: 10.1002/chem.202104420.

(40) Bila, G.; Schneider, M.; Peshkova, S.; Krajnik, B.; Besh, L.; Lutsyk, A.; Matsyura, O.; Bilyy, R. Novel Approach for Discrimination of Eosinophilic Granulocytes and Evaluation of Their Surface Receptors in a Multicolor Fluorescent Histological Assessment. *Ukr. Biochem. J.* **2020**, *92* (2), 99–106.

(41) Instrumentation for Fluorescence Spectroscopy. In *Principles of Fluorescence Spectroscopy*; Lakowicz, J. R., Ed.; Springer: Boston, MA, 2006; Vol. 33. DOI: 10.1007/978-0-387-46312-4\_2.

(42) McKerrrow, A. J.; Buncel, E.; Kazmaier, P. M. Aggregation of Squaraine Dyes: Structure–Property Relationships and Solvent Effects. *Can. J. Chem.* **1995**, *73* (10), 1605–1615.

(43) Peyratout, C.; Daehne, L. Aggregation of Thiocyanine Derivatives on Polyelectrolytes. *Phys. Chem. Chem. Phys.* **2002**, *4* (13), 3032–3039.

(44) Behera, G. B.; Behera, P. K.; Mishra, B. K. Cyanine Dyes: Self Aggregation and Behaviour in Surfactants: A Review. *J. Surf. Sci. Technol.* **2007**, *23* (1–2), 1–31.

(45) Suzuki, M.; Hanabusa, K. Polymer Organogelators That Make Supramolecular Organogels through Physical Cross-Linking and Self-Assembly. *Chem. Soc. Rev.* **2010**, *39* (2), 455–463.

(46) De Feyter, S.; De Schryver, F. C. Two-Dimensional Supramolecular Self-Assembly Probed by Scanning Tunneling Microscopy. *Chem. Soc. Rev.* **2003**, *32* (3), 139–150.

(47) Chen, H.; Farahat, M. S.; Law, K.-Y.; Whitten, D. G. Aggregation of Surfactant Squaraine Dyes in Aqueous Solution and Microheterogeneous Media: Correlation of Aggregation Behavior with Molecular Structure. *J. Am. Chem. Soc.* **1996**, *118* (11), 2584–2594.

(48) Herz, A. H. Aggregation of Sensitizing Dyes in Solution and Their Adsorption onto Silver Halides. *Adv. Colloid Interface Sci.* **1977**, *8* (4), 237–298.

(49) Chen, G.; Sasabe, H.; Lu, W.; Wang, X.-F.; Kido, J.; Hong, Z.; Yang, Y. J-Aggregation of a Squaraine Dye and Its Application in Organic Photovoltaic Cells. *J. Mater. Chem. C* **2013**, *1* (40), 6547.

(50) Kobayashi, T. *J-Aggregates*; World Scientific, 1996. DOI: 10.1142/3168.

(51) Kaczmarek-Kedziera, A.; Kędziera, D. Molecular Aspects of Squaraine Dyes Aggregation and Its Influence on Spectroscopic Properties. *Theor. Chem. Acc.* **2016**, *135* (9), 214.

(52) Cleaves, H. J. Carboxylic Acid. In *Encyclopedia of Astrobiology*; Springer: Berlin Heidelberg: Berlin, Heidelberg, 2011; pp 249–250. DOI: 10.1007/978-3-642-11274-4\_238.

(53) Würthner, F.; Kaiser, T. E.; Saha-Möller, C. R. J-Aggregates: From Serendipitous Discovery to Supramolecular Engineering of Functional Dye Materials. *Angew. Chemie Int. Ed.* **2011**, *50* (15), 3376–3410.

(54) Williams, R. J.; Lipowska, M.; Patonay, G.; Strekowski, L. Comparison of Covalent and Noncovalent Labeling with Near-Infrared Dyes for the High-Performance Liquid Chromatographic Determination of Human Serum Albumin. *Anal. Chem.* **1993**, *65* (5), 601–605.

(55) Saikiran, M.; Pandey, S. S.; Hayase, S.; Kato, T. Photophysical Characterization and BSA Interaction of Direct Ring Carboxy Functionalized Symmetrical Squaraine Dyes. *J. Phys. Conf. Ser.* **2017**, *924* (1), 012006.

(56) Turbay, M. B. E.; Rey, V.; Argañaraz, N. M.; Morán Vieyra, F. E.; Aspée, A.; Lissi, E. A.; Borsarelli, C. D. Effect of Dye Localization and Self-Interactions on the Photosensitized Generation of Singlet Oxygen by Rose Bengal Bound to Bovine Serum Albumin. *J. Photochem. Photobiol. B Biol.* **2014**, *141*, 275–282.

(57) Chuang, V. T. G.; Otagiri, M. Stereoselective Binding of Human Serum Albumin. *Chirality* **2006**, *18* (3), 159–166.

(58) Zhong, D.; Douhal, A.; Zewail, A. H. Femtosecond Studies of Protein–Ligand Hydrophobic Binding and Dynamics: Human Serum Albumin. *Proc. Natl. Acad. Sci. U. S. A.* **2000**, *97* (26), 14056–14061.

(59) Jisha, V. S.; Arun, K. T.; Hariharan, M.; Ramaiah, D. Site-Selective Interactions: Squaraine Dye–Serum Albumin Complexes with Enhanced Fluorescence and Triplet Yields. *J. Phys. Chem. B* **2010**, *114* (17), 5912–5919.

(60) Pandey, R. K.; Constantine, S.; Tsuchida, T.; Zheng, G.; Medforth, C. J.; Aoudia, M.; Kozyrev, A. N.; Rodgers, M. A. J.; Kato, H.; Smith, K. M.; Dougherty, T. J. Synthesis, Photophysical Properties, in Vivo Photosensitizing Efficacy, and Human Serum Albumin Binding Properties of Some Novel Bacteriochlorins. *J. Med. Chem.* **1997**, *40* (17), 2770–2779.

(61) Yamasaki, K.; Maruyama, T.; Kragh-Hansen, U.; Otagiri, M. Characterization of Site I on Human Serum Albumin: Concept about the Structure of a Drug Binding Site. *Biochim. Biophys. Acta - Protein Struct. Mol. Enzymol.* **1996**, *1295* (2), 147–157.

(62) Jisha, V. S.; Arun, K. T.; Hariharan, M.; Ramaiah, D. Site-Selective Binding and Dual Mode Recognition of Serum Albumin by a Squaraine Dye. *J. Am. Chem. Soc.* **2006**, *128* (18), 6024–6025.

(63) Xu, H.; Schikora, M.; Sisa, M.; Daum, S.; Klemt, I.; Janko, C.; Alexiou, C.; Bila, G.; Bilyy, R.; Gong, W.; Schmitt, M.; Sellner, L.; Mokhir, A. An Endoplasmic Reticulum Specific Pro-amplifier of Reactive Oxygen Species in Cancer Cells. *Angew. Chemie Int. Ed.* **2021**, *60* (20), 11158–11162.

(64) Zhang, R.; Qin, X.; Kong, F.; Chen, P.; Pan, G. Improving Cellular Uptake of Therapeutic Entities through Interaction with Components of Cell Membrane. *Drug Delivery* **2019**, *26* (1), 328–342.

(65) Matsson, P.; Kihlberg, J. How Big Is Too Big for Cell Permeability? *J. Med. Chem.* **2017**, *60* (5), 1662–1664.

(66) Matsson, P.; Doak, B. C.; Over, B.; Kihlberg, J. Cell Permeability beyond the Rule of 5. *Adv. Drug Delivery Rev.* **2016**, *101*, 42–61.

(67) Bennion, B. J.; Be, N. A.; McNerney, M. W.; Lao, V.; Carlson, E. M.; Valdez, C. A.; Malfatti, M. A.; Enright, H. A.; Nguyen, T. H.; Lightstone, F. C.; Carpenter, T. S. Predicting a Drug's Membrane Permeability: A Computational Model Validated With in Vitro Permeability Assay Data. *J. Phys. Chem. B* **2017**, *121* (20), 5228–5237.

(68) Milanetti, E.; Raimondo, D.; Tramontano, A. Prediction of the Permeability of Neutral Drugs Inferred from Their Solvation Properties. *Bioinformatics* **2016**, *32* (8), 1163–1169.

(69) Kokate, A.; Li, X.; Jasti, B. Effect of Drug Lipophilicity and Ionization on Permeability Across the Buccal Mucosa: A Technical Note. *AAPS PharmSciTech* **2008**, *9* (2), 501–504.

(70) Daina, A.; Michielin, O.; Zoete, V. SwissADME: A Free Web Tool to Evaluate Pharmacokinetics, Drug-Likeness and Medicinal Chemistry Friendliness of Small Molecules. *Sci. Rep.* **2017**, *7* (1), 42717.